Journal of Alloys and Compounds 488 (2009) 138–143

Contents lists available at ScienceDirect

Journal of Alloys and Compounds

journal homepage: www.elsevier.com/locate/jallcom

Determination of interfacial energies in the Al–Ag and Sn–Ag alloys by using Bridgman type solidification apparatus

S. Engin[a], U. Böyük[b], N. Maraşlı[c,*]

[a] Institute of Science and Technology, Department of Physics, Erciyes University, Kayseri, Turkey
[b] Department of Science Education, Education Faculty, Erciyes University, Kayseri, Turkey
[c] Department of Physics, Faculty Arts & Sciences, Erciyes University, 38039 Kayseri, Turkey

ARTICLE INFO

Article history:
Received 23 July 2009
Received in revised form 21 August 2009
Accepted 27 August 2009
Available online 8 September 2009

Keywords:
Metals and alloys
Surfaces and interfaces
Crystal growth
Phase transitions

ABSTRACT

The equilibrated grain boundary groove shapes in the Al–Ag and Sn–Ag eutectic systems for the first time were observed in a linear temperature gradient by using a Bridgman type directional solidification apparatus. Gibbs–Thomson coefficient, solid–liquid interfacial energy and grain boundary energy for solid ζ (Ag–42 at.% Al), solid Al solution (Al–23.8 at.% Ag) and solid Sn were determined from observed grain boundary groove shapes. The results obtained in present work have been compared with the experimental results obtained in previous works for similar solid phases in the binary and ternary alloys.

1. Introduction

The solid–liquid interfacial energy, σ_{SL}, is recognized to play a key role in a wide range of metallurgical and materials phenomena from wetting [1] and sintering through to phase transformations and coarsening [2]. Thus, a quantitative knowledge of σ_{SL} values is necessary. The measurement of σ_{SL} in pure materials and alloys is difficult. Recently, a technique for the quantification of interfacial free energy from the grain boundary groove shape has been established [3–29]. Observation of groove shape in a thermal gradient can be used to determine the interfacial energy, in dependent of the grain boundary energy because the interface near the groove must everywhere satisfy:

$$\Delta T_r = \left[\frac{1}{\Delta S^*}\right]\left[\left(\sigma_{SL} + \frac{d^2\sigma_{SL}}{dn_1^2}\right)\kappa_1 + \left(\sigma_{SL} + \frac{d^2\sigma_{SL}}{dn_2^2}\right)\kappa_2\right] \quad (1)$$

where ΔT_r is the curvature undercooling, ΔS^* is the entropy of fusion per unit volume, $n = (n_x, n_y, n_z)$ is the interface normal, κ_1 and κ_2 are the principal curvatures, and the derivatives are taken along the directions of principal curvature. Thus, the curvature undercooling is a function of curvature, interfacial free energy and the second derivative of the interfacial free energy. Eq. (1) is valid only if the interfacial free energy per unit area is equal to surface tension per unit length, $\sigma_{SL} = \gamma$. When surface energy differs from surface tension, the problem is more complicated and the precise modification of the Gibbs–Thomson equation is not yet established [30]. When the solid–liquid interfacial free energy is isotropic, Eq. (1) becomes:

$$\Delta T_r = \frac{\sigma_{SL}}{\Delta S^*}\left(\frac{1}{r_1} + \frac{1}{r_2}\right) \quad (2)$$

where r_1 and r_2 are the principal radii of curvature. For the case of a planar grain boundary intersecting a planar solid–liquid interface, $r_2 = \infty$ and the Eq. (2) becomes:

$$\Gamma = r\,\Delta T_r = \frac{\sigma_{SL}}{\Delta S^*}, \quad (3)$$

where Γ is the Gibbs–Thomson coefficient. This equation is called the Gibbs–Thomson relation [3]. At present the most powerful method to measure solid–liquid interface energy experimentally uses the Gibbs–Thomson equation. Measurements of solid–liquid interfacial energies were made for some transparent organic materials [3–13].

Gündüz and Hunt [14] have developed an apparatus to observe the equilibrated grain boundary groove shapes in opaque binary eutectic systems. The details of apparatus and experimental procedures are given in Ref. [14]. Gündüz and Hunt [14] have also developed a finite difference model to determine the Gibbs–Thomson coefficient from observed grain boundary groove shapes. If the grain boundary groove shape, the temperature gradient in the solid, G_S and the ratio of thermal conductivity of the equilibrated liquid phase to solid phase, $R = K_L/K_S$ are known or measured the value of the Gibbs–Thomson coefficient is then

* Corresponding author. Tel.: +90 352 4374901x33114; fax: +90 352 4374933.
E-mail address: marasli@erciyes.edu.tr (N. Maraşlı).

0925-8388/$ – see front matter © 2009 Elsevier B.V. All rights reserved.
doi:10.1016/j.jallcom.2009.08.156

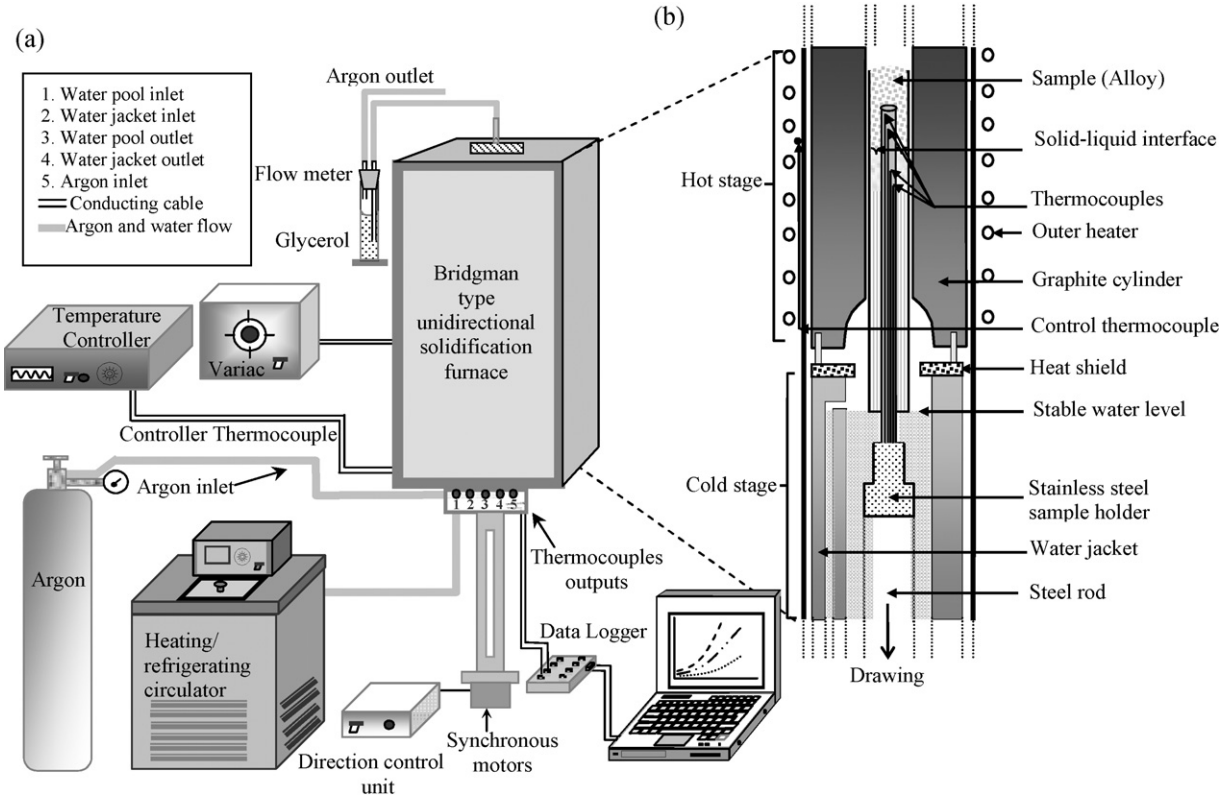

Fig. 1. (a) Block diagram of the experimental setup and (b) the details of the Bridgman type directional solidification furnace.

obtained with the Gündüz and Hunt numerical method [14]. The solid–liquid interfacial energy measurements for some metallic binary and ternary eutectic based systems were made in Refs. [14–23].

Bayender et al. [24] designed a horizontal temperature gradient stage to directly observe equilibrated grain boundary groove shape for transparent materials. They applied Gündüz and Hunt's numerical method to determine Gibbs–Thomson coefficients, solid–liquid interface energies and grain boundary energies. Measurements of the solid–liquid interface energies for some transparent organic binary systems were also made in Refs. [24–28].

As described in Refs. [14–23], the experimental process to observe the equilibrated grain boundary groove shapes in opaque binary alloys with the radial heat flow apparatus is very hard, and needs a long period, usually more than one week. The experimental setup is also very complicate and needs a very sensitive temperature control. There was also a working temperature range limitation on the experimental technique. More recently, Böyük et al. [29] have developed an experimental technique to observe the equilibrated grain boundary groove shapes in opaque alloys. In the experimental technique, a constant linear temperature gradient on the sample was established by heating from one side of the sample and cooling the other side of the sample at 273 K with a heating/refrigerating circulating bath in a Bridgman type directional solidification apparatus and annealed for few hours (4–6 h). At the end of the annealing time the specimen was rapidly quenched by just pulling it into the water cooled bath. This experimental technique is very simple, useful and also can be used for metallic alloys, which have high melting temperature (especially higher than 973 K).

Some thermo-physical properties such as Gibbs–Thomson coefficient, solid–liquid and grain boundary energies in the Al–Ag and Sn–Ag eutectic systems have not been well known. This sort of thermo-physical properties could be of use to people doing comparison between experimentally observed solidification morphology and predictions from theoretical models. Thus the aims of the present work were to observe the grain boundary groove shapes in the Al–Ag and Sn–Ag alloys with a Bridgman type solidification apparatus and determine the Gibbs–Thomson coefficients, solid–liquid interfacial energies and grain boundary energies in the Al–Ag and Sn–Ag alloys from the observed grain boundary groove shapes.

2. Experimental procedure

2.1. Experimental apparatus

As mentioned above, Böyük et al. [29] have observed the equilibrated grain boundary groove shapes in opaque alloys by using the Bridgman type directional solidification apparatus. In the present work, a similar experimental technique was used to observe the equilibrated grain boundary groove shapes in the Al–Ag and Sn–Ag alloys. Block diagram of experimental setup and the details of Bridgman type directional solidification apparatus are shown in Fig. 1.

2.2. Sample production

A thin-walled graphite crucible, 12.0 mm OD × 8.0 mm ID × 150 mm in length was made by drilling out a graphite rod, 12.0 mm diameter and 600 mm in length. A hole, 1.5 mm in diameter was drilled at the bottom of crucible for thermocouples insulation as shown in Fig. 1b.

The phase diagrams of Ag–Al and Sn–Ag binary systems are given in Ref. [31]. The structures of solid phases with the composition range of 42–100 at.% Al in Ag–Al binary system consist of solid ζ and solid Al solution phases at the eutectic temperature and the compositions of solid ζ, and Al solution phases are 42 at.% Al and 76.2 at.% Al [31], respectively. The solid solubility of Ag in Sn is less than 0.09 at.% Ag at 210 °C [31]. Thus the compositions of alloys were chosen to be Ag–43 at.% Al, Al–23.8 at.% Ag and Sn–1 at.% Ag to grow the single solid ζ (Ag–42 at.% Al), solid Al solution (Al–23.8 at.% Ag) and solid Sn on the eutectic structures.

Alloys were prepared in a vacuum furnace by using 99.9% pure silver and 99.999% pure aluminum and 99.99% pure tin. After stirring, the molten alloy was poured into a graphite crucible held in a specially constructed casting furnace at approximately 50 K above the melting point of the alloy. The molten metal was then directionally solidified from bottom to top to ensure that the crucible was completely full.

Table 1
Temperature gradients of solid and liquid phases and thermal conductivity ratios of equilibrated liquid phase to solid phase in the Ag–Al and Sn–Ag binary eutectic alloy at their melting temperature.

Alloy	Phases	Melting temperature (K)	G (K/mm)	$R = G_S/G_L$
Ag–Al	Liquid (Al–37.5 at.% Ag)	839	7.21	1.03
	Solid ζ (Ag–42 at.% Al)		7.43	
	Liquid (Al–37.5 at.% Ag)	839	5.84	0.67
	Solid Al (Al–23.8 at.% Ag)		3.89	
Sn–Ag	Liquid (Sn–3.84 at.% Ag)	494	2.23	1.16
	Solid Sn (Sn–0.09 at.% Ag)		2.60	

The specimen was then positioned in a graphite cylinder (300 mm in length 20 mm ID and 40 mm OD) held in a Bridgman type furnace to get a uniform temperature distribution in the horizontal direction of the specimen as shown in Fig. 1b and annealed in a linear temperature gradient for a sufficient period. The single solid phase grew on the casting phase during the annealing period. The annealing time for these alloys was 4–6 h. During the annealing period, the temperatures on the specimen were continuously recorded by four stationary thermocouples with a data logger via computer. The temperature on the sample was stable to about ± 0.05 K for hours. At the end of the annealing time the specimen was rapidly quenched by just pulling it into the water cooled bath. Detail of experimental procedure is given in Ref. [29].

2.3. Measurements of the coordinates of equilibrated grain boundary groove shapes

The quenched sample was removed from the graphite crucible and cut longitudinally into 8 mm length around the solid–liquid interface. The longitudinal section was ground flat with 180 grit Sic paper and then cold mounted with epoxy-resin. After grinding and polishing, the samples of Ag–Al and Sn–Ag alloys were etched with Keller's etch (1.5% HCl–0.5% HF–2.5% HNO_3–95.5% H_2O) for 10–15 s and 2 g CrO_3–10 ml g H_2SO_4 in 90 ml water for 2–3 s, respectively.

The equilibrated grain boundary groove shapes were photographed with a *CCD* digital camera placed in conjunction with a light optical microscope. A graticule ($200 \times 0.01 = 2$ mm) was also photographed using the same objective. The photographs of the equilibrated grain boundary groove shapes and the graticule were superimposed on one another using software so that accurate measurement of the groove coordinate points on the groove shapes could be made.

The coordinates of cusp x', y' from the metallographic section must be transformed to x, y coordinates. Maraşlı and Hunt [15] devised a geometrical method to make appropriate corrections to the groove shapes and the detail of geometrical method is given in Ref. [15]. Geometrical correction for the groove coordinates was made by following Maraşlı and Hunt's [15] geometrical method. The coordinates of equilibrated grain boundary groove shapes were measured with an optical microscope to an accuracy of ±10 μm. The thickness of the sample (2–2.5 cm lengths) for geometrical correction was measured with a digital micrometer which has ±1 μm resolution. Thus the uncertainty in the measurements of equilibrated grain boundary coordinates was less than 0.2% [29].

2.4. The temperature gradient measurement

The temperature of Bridgman type furnace was controlled to an accuracy of ± 0.1 K. The temperature in the specimen was measured with 0.25 mm diameter insulated four K-type thermocouples fixed within the sample with spacing of 4–6 mm as shown in Fig. 1b. During the annealing period, the temperatures on the solid and liquid phases were continuously recorded by the stationary thermocouples with a data logger via computer. The temperature gradients ($G = \Delta T/\Delta X$) in the liquid and solid phases for each sample were determined using the measured values of ΔT and ΔX and given in Table 1. Details of the measurement of ΔT and ΔX are given in Ref. [29]. The estimated error in the measurements of temperature gradient is about 4% [29].

2.5. Thermal conductivity ratio of equilibrated liquid phase to solid phase

The thermal conductivity ratio of equilibrated eutectic liquid phase to solid phase, $R = K_{L(\text{eutectic liquid})}/K_S$ must be known or measured to evaluate the Gibbs–Thomson coefficients with the present numerical method.

At the steady-state condition, the heat flow away from the interface through the solid phase must balance that of the liquid phase so that the thermal conductivity ratio of liquid phase to solid phase, R is given by

$$R = \frac{K_L}{K_S} = \frac{G_S}{G_L}, \tag{4}$$

where G_L and G_S are the temperature gradients of liquid and solid phases, respectively at the steady-state condition. The temperature gradients on the solid and liquid phase were measured at the steady-state condition. The values of G_L, G_S and R used in determination of Gibbs–Thomson coefficients are given in Table 1. In present work, the value of R was determined from the temperature gradient measurements on the solid and liquid phases in the same time with grain boundary groove shape observation by using the Bridgman type directional solidification apparatus.

3. Results and discussion

3.1. Determination of Gibbs–Thomson coefficient

If the thermal conductivity ratio of the equilibrated liquid phase to the solid phase, the coordinates of the grain boundary groove shapes and the temperature gradient of the solid phase are known, the Gibbs–Thomson coefficient (Γ) can be obtained using the numerical method described in detail Ref. [14].

The experimental error in the determination of Gibbs–Thomson coefficient is the sum of experimental errors in the measurements of the temperature gradient in the solid and liquid phases and groove coordinates. Thus the total error in the determination of Gibbs–Thomson coefficient is about 8% [29].

3.1.1. Solid ζ (Ag–42 at.% Al) phase in equilibrium with the eutectic Ag–Al liquid interface

The Gibbs–Thomson coefficients for solid ζ (Ag–42 at.% Al) in equilibrium with the eutectic Ag–Al liquid were determined with the present numerical model by using ten equilibrated grain boundary groove shapes and given in Table 2. Typical grain boundary groove shapes for solid ζ (Ag–42 at.% Al) in equilibrium with the Ag–Al eutectic liquid are shown in Fig. 2a and b. The average value of Γ from Table 2 is obtained to be $(8.40 \pm 0.67) \times 10^{-8}$ Km for solid ζ (Ag–42 at.% Al).

3.1.2. Solid Al solution in equilibrium with the eutectic Al–Ag liquid interface

The Gibbs–Thomson coefficients for solid Al solution (Al–23.8 at.% Ag) in equilibrium with the eutectic Al–Ag liquid were determined with the present numerical model by using 10 equilibrated grain boundary groove shapes and are given in

Table 2
Gibbs–Thomson coefficient for solid ζ in equilibrium with the Ag–37.5 at.% Al liquid. The subscripts LHS and RHS refer to left hand side and right hand side of groove, respectively.

Grove no.	α°	β°	Gibbs–Thomson coefficient	
			$\Gamma_{LHS} \times 10^{-8}$ (Km)	$\Gamma_{RHS} \times 10^{-8}$ (Km)
a	4.6	26.4	8.28	8.34
b	6.7	34.6	8.44	8.46
c	4.2	11.6	8.56	8.29
d	5.8	32.5	8.21	8.39
e	4.4	18.7	8.26	8.38
f	2.3	28.2	8.50	8.42
g	9.4	11.3	8.36	8.48
h	6.4	23.8	8.32	8.35
i	2.8	16.5	8.31	8.40
j	3.9	19.9	8.50	8.68
			$\bar{\Gamma}$ $(8.40 \pm 0.67) \times 10^{-8}$ Km	

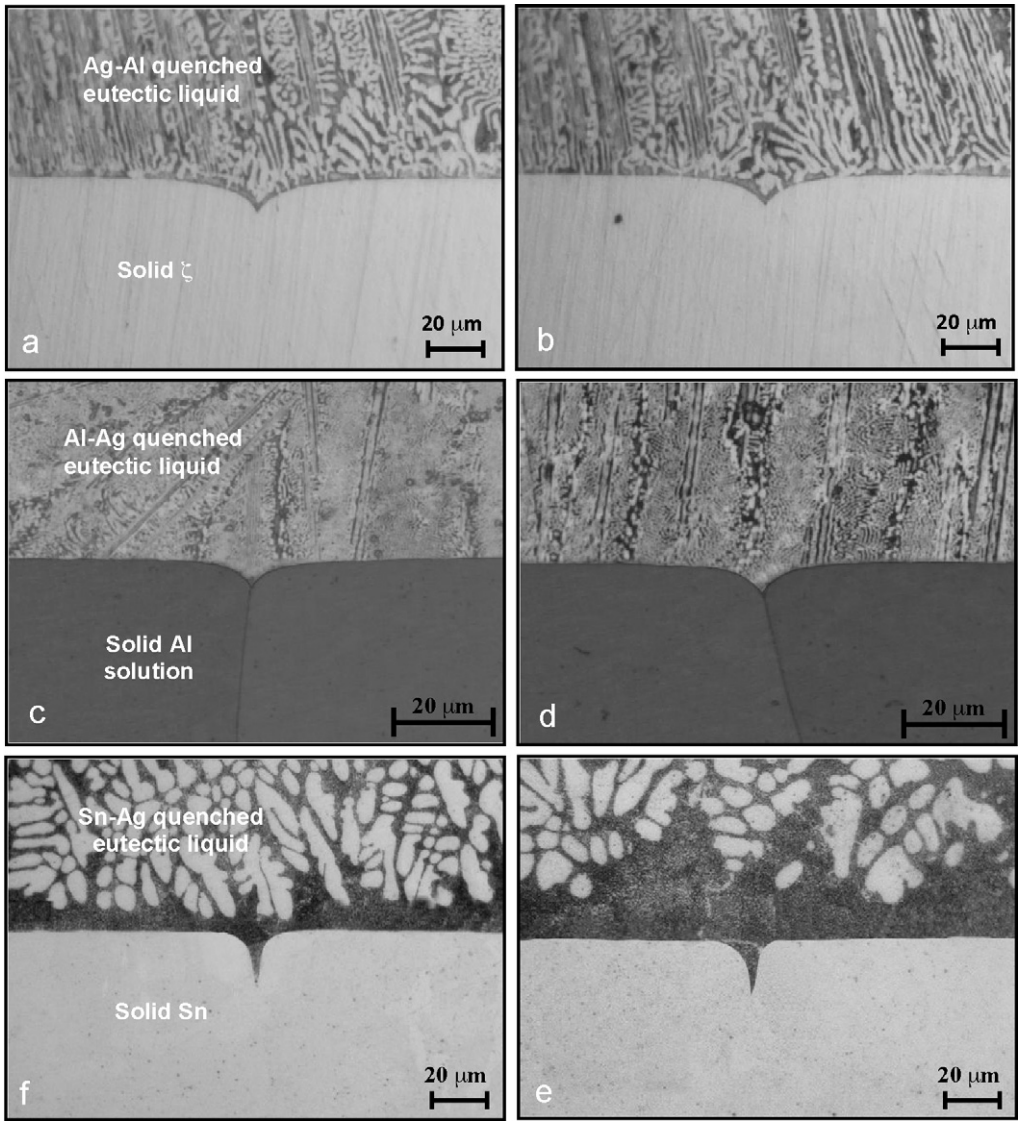

Fig. 2. Typical grain boundary groove shapes observed with a Bridgman type directional solidification apparatus in the Ag–Al and Sn–Ag alloys.

Table 3. Typical grain boundary groove shapes for solid Al solution in equilibrium with the eutectic Al–Ag liquid are shown in Fig. 2c and d. The average value of Γ from Table 3 is obtained to be $(20.4 \pm 1.6) \times 10^{-8}$ Km for solid Al solution.

Table 3
Gibbs–Thomson coefficient for solid Al solution in equilibrium with the Ag–37.5 at.% Al liquid. The subscripts LHS and RHS refer to left hand side and right hand side of groove, respectively.

Grove no.	α°	β°	Gibbs–Thomson coefficient	
			$\Gamma_{LHS} \times 10^{-8}$ (Km)	$\Gamma_{RHS} \times 10^{-8}$ (Km)
a	5.2	10.4	18.9	21.2
b	6.3	22.5	21.6	20.7
c	4.2	12.7	19.7	21.4
d	3.8	31.5	21.5	19.3
e	5.4	20.9	20.8	20.8
f	3.3	32.2	19.5	19.4
g	2.4	15.3	20.4	18.9
h	6.4	24.8	20.9	19.3
i	3.9	11.9	21.3	21.7
j	2.8	16.3	19.4	21.3
			$\bar{\Gamma}$ $(20.4 \pm 1.6) \times 10^{-8}$ Km	

3.1.3. Solid Sn in equilibrium with the eutectic Sn–Ag liquid interface

The Gibbs–Thomson coefficients for solid Sn in equilibrium with the eutectic Sn–Ag liquid were also determined with the present numerical model by using 10 equilibrated grain boundary groove shapes and given in Table 4. Typical grain boundary groove shapes for solid Sn in equilibrium with the eutectic Sn–Ag liquid are also shown in Fig. 2e and f. The average value of Γ from Table 4 is obtained to be $(8.86 \pm 0.71) \times 10^{-8}$ Km for solid Sn.

3.2. Determination of entropy of fusion per unit volume

It is also necessary to know the entropy of fusion per unit volume, ΔS_f for the solid phases to determine the solid–liquid interfacial energy. The entropy change per unit volume for an alloy is given by [14]:

$$\Delta S_f = \frac{RT_M}{m_L V_S} \frac{C_S - C_L}{(1 - C_L) C_L}, \quad (5)$$

where C_S and C_L are the solid and liquid compositions, respectively, R is the gas constant, T_M is the melting temperature, V_S is the molar volume of solid phase and m_L is the slope of liquidus. The molar

Table 4
Gibbs–Thomson coefficient for solid Sn in equilibrium with the Sn–3.84 at.% Ag liquid. The subscripts LHS and RHS refer to left hand side and right hand side of groove, respectively.

Grove no.	α°	β°	Gibbs–Thomson coefficient	
			$\Gamma_{LHS} \times 10^{-8}$ (Km)	$\Gamma_{RHS} \times 10^{-8}$ (Km)
a	5.6	21.6	9.48	9.56
b	6.9	27.4	8.63	8.83
c	5.8	18.6	9.13	8.19
d	4.7	15.5	8.39	8.27
e	4.4	11.7	8.26	9.45
f	3.2	28.2	8.34	8.42
g	9.4	12.4	9.42	9.32
h	8.3	32.1	8.88	8.21
i	4.6	14.9	8.56	9.48
j	3.9	19.9	9.52	8.68
			$\bar{\Gamma}$ $(8.86 \pm 0.71) \times 10^{-8}$ Km	

volume of solid is expressed as

$$V_S = V_c N_a \frac{1}{n}, \quad (6)$$

where V_c is the volume of the unit cell, N_a is the Avogadro's number and n is the number of molecules per unit cell.

The values of the relevant constant used in the determination of entropy change per unit volume are given in Table 5. The error in the determined entropy change of fusion per unit volume is estimated to be about 5% [33].

3.3. Determination of solid–liquid interfacial energies in the Al–Ag and Ag–Sn alloys

If the values of Γ and ΔS_f are known, the value of solid–liquid interfacial energy, σ_{SL} can be determined from Eq. (3). The experimental error in the determination of solid–liquid interfacial energy is the sum of experimental errors of the Gibbs–Thomson coefficient and the entropy change of fusion per unit volume. Thus, the total experimental error of the solid–liquid interfacial energy determination in the present work is about 13%. The solid–liquid interfacial energy of solid ζ (Ag–42 at.% Al) in equilibrium with the eutectic Ag–Al liquid, solid Al solution (Al–23.8 at.% Ag) in equilibrium with the eutectic Al–Ag liquid and solid Sn in equilibrium with the eutectic Sn–Ag liquid was determined to be $(64.68 \pm 8.41) \times 10^{-3}$, $(166.32 \pm 21.62) \times 10^{-3}$ and $(113.41 \pm 14.74) \times 10^{-3}$ J m^{-2}, respectively by using the values of Γ and ΔS_f for each phases.

3.4. Calculation of grain boundary energy of solid ζ, solid Al solution and solid Sn

If the grains on either side of the interface are the same phase then the grain boundary energy can be expressed by

$$\sigma_{gb} = 2\sigma_{SL} \cos\theta, \quad (7)$$

where $\theta = (\theta_A + \theta_B)/2$ is the angle that the solid–liquid interfaces make with the y axis. The angles, θ_A and θ_B were obtained from the cusp coordinates, x, y using a Taylor expansion for parts at the base of the groove. According to Eq. (7), the value of σ_{gb} should be smaller or equal to twice of solid–liquid interface energy, i.e. $\sigma_{gb} \leq 2\sigma_{SL}$.

The estimated error in determination of θ angles was found to be 2%. Thus the total experimental error in the resulting grain boundary energy is about 15%. The values of the grain boundary energy for solid ζ (Ag–42 at.% Al), solid Al solution (Al–23.8 at.% Ag) and solid Sn were found to be $(119.94 \pm 17.99) \times 10^{-3}$, $(329.40 \pm 49.41) \times 10^{-3}$ and $(222.96 \pm 33.44) \times 10^{-3}$ J m^{-2}, respectively by using the values of σ_{SL} and θ for each phase in Eq. (6).

The role of interfacial energy anisotropy is considered to play a critical role in many phase transformations. Solid ζ (Ag–42 at.% Al), solid Al solution (Al–23.8 at.% Ag) and solid Sn phases have the rough solid–liquid interfaces. The anisotropy of solid–liquid interfacial energy for rough solid–liquid interfaces in metals is known to be small, in order of 1–2% [34]. In the present work, the solid–liquid interface energy was assumed to be isotropic and a mean values of solid–liquid interfacial energy were obtained.

A comparison of the values of Gibbs–Thomson coefficient (Γ), solid–liquid interface energy (σ_{SL}) and grain boundary energy (σ_{gb}) for solid ζ, solid Al solution and solid Sn obtained in the present work with the values of Γ, σ_{SL} and σ_{gb} for similar solid phases

Table 5
Some thermo-physical properties in the Ag–Al and Sn–Ag binary alloys.

Alloys	Single solid phase C_S	Quenched liquid phase C_L	f(C)	T_m (K)	$V_s \times 10^{-6}$ (m^3)	$m_L \times 10^2$ (K/at.%)	$\Delta S_f \times 10^6$ (J/K m^3)
Ag–Al	Ag–42 at.% Al [31]	Al–37.5 at.% Ag [31]	−0.87	839	9.88	−7.97 [31]	0.77 ± 0.038
	Al–23.8 at.% Ag [31]	Al–37.5 at.% Ag [31]	0.58	839	9.9068 [32]	5.04 [31]	0.82 ± 0.042
Sn–Ag	Sn–0.09 at.% Ag [31]	Sn–3.84 at.% Ag [31]	−1.62	494	16.2	3.21 [31]	1.28 ± 0.064

$f(C) = C_S - C_L/[(1 - C_L)C_L]$.

Table 6
A comparison of the values of Γ, σ_{SL} and σ_{gb} for Ag–Al and Sn–Ag binary alloys obtained in the present work with the values of Γ, σ_{SL} and σ_{gb} obtained in previous works.

System	Solid phase	Liquid phase	Temperature (K)	$\Gamma \times 10^{-8}$ (Km)	$\sigma_{SL} \times 10^{-3}$ (J m^{-2})	$\sigma_{gb} \times 10^{-3}$ (J m^{-2})
Ag–Al	ζ (Ag–42 at.% Al)	Al–37.5 at.% Ag	839	8.4 ± 0.67 [PW]	64.68 ± 8.41 [PW]	119.94 ± 17.99 [PW]
Al–Si	Al (Al–1.59 at.% Cu)	Al–12.1 at.% Si	850	19.6 ± 1.6 [14]	168.95 ± 21.96 [14]	336.50 ± 47.11 [14]
Al–Mg	Al (Al–18.9 at.% Mg)	Al–37.4 at.% Mg	723	13.0 ± 1.0 [35]	149.20 ± 19.40 [35]	295 ± 41 [35]
Al–$CuAl_2$	Al (Al–2.5 at.% Cu)	Al–17.3 at.% Cu	821	23.6 ± 1.6 [15]	160.01 ± 19.20 [15]	234.70 ± 45.46 [15]
Al–$NiAl_3$	Al (Al–0.023 at.% Ni)	Al–3.06 at.% Ni	913	18.6 ± 1.3 [15]	171.56 ± 20.58 [15]	336.50 ± 47.11 [15]
Al–Ti	Al (Al–0.186 at.% Ti)	Al–0.0169 at.% Ti	938	13.1 ± 0.9 [15]	174.62 ± 20.95 [15]	335.14 ± 46.92 [15]
Al–Cu–Ag	Al (Al–16.42 at.% Ag–4.97 at.% Cu)	Al–16.57 at.% Ag–11.87 at.% Cu	775	6.3 ± 1.4 [23]	67 ± 15 [23]	–
Al–Cu–Ag	Al (Al–16.42 at.% Ag–4.97 at.% Cu)	Al–16.57 at.% Ag–11.87 at.% Cu	775	22.9 ± 1.6 [36]	137.40 ± 16.49 [36]	268.20 ± 34.87 [36]
Al–Ag	Al (Al–23.8 at.% Ag)	Al–37.5 at.% Ag	839	20.4 ± 1.6 [PW]	166.32 ± 21.62 [PW]	329.40 ± 49.41 [PW]
Sn–In–Bi	Sn (Sn–40.14 at.% In–16.11 at.% Bi)	In–21.23 at.% Bi–19.04 at.% Sn	332	7.68 ± 0.39 [37]	144.4 ± 14.4 [37]	284.6 ± 31.3 [37]
Sn–Pb	Sn (Sn–1.45 at.% Pb)	Sn–26.1 at.% Pb	456	7.85 ± 0.63 [14]	132.43 ± 5.0 [14]	262.77 ± 36.79 [14]
Sn–Cd	Sn (Sn–5.83 at.% Cd)	Sn–33.46 at.% Cd	450	7.3 ± 0.6 [38]	146 ± 11 [38]	283 ± 40 [38]
Sn–Ag	Sn (Sn–0.09 at.% Ag)	Sn–3.84 at.% Ag	494	8.86 ± 0.71 [PW]	113.41 ± 14.74 [PW]	222.96 ± 33.44 [PW]

PW: present work.

determined in previous works is given in Table 6. As can be seen from Table 6, the resulting values of Gibbs–Thomson coefficient (Γ), solid–liquid interfacial energy (σ_{SL}) and grain boundary energy (σ_{gb}) for solid Al solution are in good agreement with the values of Γ, σ_{SL} and σ_{gb} obtained with in previous works in the limits of experimental errors except the values Γ, σ_{SL} and σ_{gb} obtained by Bulla et al. [23]. The statistical fluctuation in their determination of Γ is about 85% [23]. As can be also seen from Table 6, the average value of Γ for solid Al solution obtained by Bulla et al. [23] is about three times smaller than the other average values of Γ for similar solid phase obtained in present and previous works. As can be also seen from Table 6, the resulting value of Γ for solid Sn is slightly bigger than the values of Γ for similar solid Sn phases but the resulting values of σ_{SL} and σ_{gb} for solid Sn phase are lower than the values of σ_{SL} and σ_{gb} for similar solid Sn phases obtained in previous works. This difference is probably due to the difference between the entropy change of fusion per unit volume for each phases. In literature, there is no any theoretical and experimental available data for solid ζ phase to make a comparison with our values.

4. Conclusion

In the present work, a linear temperature gradient on the vertical sample was established by heating from one end of sample and cooling the other end at 280 K with a heating/refrigerating circulating bath in a Bridgman type directional solidification apparatus. The sample was melted and annealed for 4–6 h in a linear temperature gradient. At the end of the annealing period, the sample was quenched by just pulling it into the water cooled bath. The equilibrated grain boundary groove shapes in Ag–Al and Sn–Ag binary alloys for the first time were observed from quenched sample. Gibbs–Thomson coefficient, solid–liquid interfacial energies and grain boundary energies for solid ζ, solid Al solution and solid Sn have been determined from the observed grain boundary groove shapes.

Acknowledgements

This project was supported by Erciyes University Scientific Research Project Unit under Contract No. FBT 09–672. The authors are grateful to Erciyes University Scientific Research Project Unit for their financial supports.

References

[1] N. Eustathopoulos, M.G. Nicholas, B. Drevet, Wettability at High Temperatures, Pergamon, Oxford, United Kingdom, 1999.
[2] J.W. Martin, R.D. Doherty, B. Cantor, Stability of Microstructure in Metallic Systems, Cambridge University Press, Cambridge, United Kingdom, 1976/1997.
[3] R.J. Schaefer, M.E. Glicksman, J.D. Ayers, Philos. Mag. 32 (1975) 725.
[4] D. Turnbull, J. Appl. Phys. 2 (1950) 1022.
[5] D.R.H. Jones, J. Mater. Sci. 9 (1974) 1.
[6] N. Eustathopoulos, Int. Met. Rev. 28 (1983) 189.
[7] G.F. Bolling, W.A. Tiller, J. Appl. Phys. 31 (1960) 1345.
[8] D.R.H. Jones, G.A. Chadwick, Philos. Mag. 22 (1970) 291.
[9] G.E. Nash, M.E. Glicksman, Philos. Mag. 24 (1971) 577.
[10] D.R.H. Jones, G.A. Chadwick, J. Cryst. Growth 11 (1971) 260.
[11] D.R.H. Jones, Philos. Mag. 27 (1978) 569.
[12] S.C. Hardy, Philos. Mag. 35 (1977) 471.
[13] N.B. Singh, M.E. Glicksman, J. Cryst. Growth 98 (1989) 573.
[14] M. Gündüz, J.D. Hunt, Acta Metall. 33 (1985) 1651.
[15] N. Maraşlı, J.D. Hunt, Acta Mater. 44 (1996) 1085.
[16] K. Keşlioğlu, N. Maraşlı, Mater. Sci. Eng. A 369 (2004) 294.
[17] K. Kes¸lioğlu, N. Maraşlı, Metall. Mater. Trans. A 35 (2004) 3665.
[18] M. Erol, N. Maraşlı, K. Keşlioğlu, M. Gündüz, Scripta Mater. 51 (2004) 131.
[19] N. Maraşlı, S. Akbulut, Y. Ocak, K. Keşlioğlu, U. Böyük, H. Kaya, E. Çadırlı, J. Phys. Condens. Matter 19 (2007) 506102.
[20] S. Akbulut, Y. Ocak, N. Maraşlı, K. Keşlioğlu, U. Böyük, E. Çadırlı, H. Kaya, Mater. Charact. 59 (2008) 1101.
[21] Y. Ocak, S. Akbulut, N. Maraslı, K. Keşlioğlu, U. Böyük, H. Kaya, E. Çadırlı, Met. Mater. Int. 14 (2008) 2.
[22] Y. Ocak, S. Akbulut, K. Keşlioğlu, N. Maraşlı, E. Çadırlı, H. Kaya, Chin. Phys. B 18 (2009) 3952.
[23] A. Bulla, C. Carreno-Bodensıek, B. Pustal, R. Berger, A. Buhrıg-Polaczek, A. Ludwıg, Metall. Mater. Trans. A 38 (2007) 1956.
[24] B. Bayender, N. Maraşlı, E. Çadırlı, H. Şişman, M. Gündüz, J. Cryst. Growth 194 (1998) 119.
[25] S. Akbulut, Y. Ocak, U. Böyük, M. Erol, K. Keşlioğlu, N. Maraşlı, J. Appl. Phys. 100 (2007) 123505.
[26] U. Böyük, K. Keslioğlu, N. Maras¸lı, J. Phys. Condens. Matter 19 (2007) 116202.
[27] Y. Ocak, S. Akbulut, K. Keşlioğlu, N. Maraşlı, J. Colloids Interf. Sci. 320 (2008) 555.
[28] Y. Ocak, S. Akbulut, K. Keşlioğlu, N. Maraşlı, J. Phys. D: Appl. Phys. 41 (2008) 065309.
[29] U. Böyük, S. Engin, N. Maraşlı, J. Alloys Compd. 476 (2009) 213.
[30] R. Trivedi, J.D. Huntderick, F.M. Hosking, R. Darrel Frear, Van Nostrand Reinhold, New York, 1993, 191.
[31] M. Hansen, Constitution of Binary Alloys, McGraw-Hill, New York, 1958.
[32] H.J. Axon, W. Hume-Rothery, Proc. R. Soc. Lond. A 193 (1948) 1.
[33] M. Tassa, J.D. Hunt, J. Cryst. Growth 34 (1976) 38.
[34] J.J. Hoyt, M. Asta, T. Haxhimali, A. Karma, R.E. Napolitano, R. Trivedi, MRS Bull. 29 (2004) 935.
[35] M. Gündüz, J.D. Hunt, Acta Metall. 37 (1989) 1839.
[36] K. Keşlioğlu, Y. Ocak, S. Akbulut, N. Maraşlı, E. Çadırlı, H. Kaya, Met. Mater. Int., (2009) in press.
[37] S. Akbulut, Y. Ocak, N. Maraşlı, K. Keşlioğlu, H. Kaya, E. Çadırlı, Mater. Charact. 60 (2009) 183.
[38] B. Saatçi, S. Çimen, H. Pamuk, M. Gündüz, J. Phys. Condens. Matter 19 (2007) 326219.